Model-based Optimization of Distributed and Renewable Energy Systems in Buildings

Paul Stadler*, Araz Ashouri, François Maréchal

Industrial Process and Energy System Engineering (IPESE), École Polytechnique Fédérale de Lausanne, CH-1951 Sion, Switzerland

Abstract

In order to fully exploit the potential of renewable energy resources (RERs) for building applications, optimal design and control of the different energy systems is a compelling challenge to address. This paper presents a two-step multi-objective optimization approach to size both thermal and electrical energy systems in regard of thermo-economic performance indicators to suit consumer and grid operator interests. Several utilities such as storage, conversion systems, and RERs are hence modelled and formulated through mixed-integer linear programming. Simultaneously, the algorithm defines the optimal operation strategy, based on a model predictive control structure, for each deterministic unit embedded within the energy management system of the building to meet the different comfort and service requirements.

The developed design framework is successfully applied on several energy systems configuration of typical Swiss building types. Different component sizes are analysed, regarding the present investment cost and the self-consumption share. In addition, this paper presents a novel optimal design criteria based on the maximum cost benefits in the view of both the consumer and the distribution network operator.

Keywords: Multi-Objective Optimization, Optimal design and control, Distributed Energy System, System Modelling, Complete building simulation

1. Highlights

- K-medoids clustering of the input data to improve computational efforts

- Advanced thermal modelling by applying discrete control-oriented models of thermo-electrical energy systems and heat cascading.

---

*Corresponding author, Phone Number: +41 21 695 82 60

Email addresses: `paul.stadler@epfl.ch` (Paul Stadler), `araz.ashouri@epfl.ch` (Araz Ashouri), `francois.marechal@epfl.ch` (François Maréchal)

Nomenclature

Acronyms

DHW	Domestic hot water
$MILP$	Mixed integer linear programming
NG	Natural gas
SH	Space heating

Roman Symbols

$\dot{\mathbf{E}}, E$	Power flow [kW]
$\dot{\mathbf{m}}$	Mass flow [kg/s]
$\dot{\mathbf{Q}}, Q$	Heat flow [kW]
$\mathbf{A}$	Aera [m^2]
$\mathbf{c}$	Energy cost [CHF/kWh]
$\mathbf{E}, E$	Electrical energy [kWh]
$\mathbf{I}, I$	Global solar irradiation [kW/m^2]
$\mathbf{Q}, Q$	Thermal energy [kWh]
$\mathbf{T}, T$	Temperature [K]
t	Continuous time index

Superscripts

$+/-$	Respectively incoming and outgoing flow/power
d	Design parameter
$loss$	Relative to losses
min/max	Relative to maximum and minimum values

Subscripts

bat	Relative to the battery stack
$build$	Relative to the building
cg	Relative to the cogeneration unit
dhw	Relative to the domestic hot water tank
$grid$	Relative to the distribution grid
hp	Relative to the heat pump
hs	Relative to the heat storage
k	Discrete time step
l	Discrete temperature level/interval
pv	Relative to the photovoltaic array
ts	Relative to the thermal solar collector array
u	Relative to the storage/conversion units
wat	Relative to the domestic water

- Holistic optimization approach providing cost and self-sufficient trade-off solutions to both the sizing and control problem.

2. Inroduction

In effort of addressing the growing energy demand while decreasing the environmental impact of power generation, the use of renewable energy resources (RERs) has been heavily promoted over the last decade. Especially small and micro-scale, distributed energy resource (DER) systems for building applications strongly expanded due to attractive incentives in form of beneficial feed-in tariffs and governmental subsidies on investments. Nevertheless, the significant power exports engendered by the large penetration of highly stochastic and low-inertia energy sources, e.g. photovoltaic (PV) systems, have pushed distribution grids to their current operating limits [1].

The resulting end of the different support plans and hence, the drop of feed-in tariffs below the grid selling price has endorsed self-consumption in the building sector. Indeed, self-consumption strongly reduces power curtailments losses and building operating costs while increasing the grid DER connection capacity, thus avoiding the need of over-hauling the entire power network. Both demand response and the use of storage systems represent two promising options to enhance on-site, self-consumption of the generated power [2]. Hence, in order to fully exploit the benefits of RERs, in view of both the grid operator and consumer interests, optimal sizing and operation of the different DER systems is of high importance. To tackle this compelling challenge, several sizing approaches have been developed to identify the optimal combination of conventional and RER based energy systems [3–5]. However, the growing integration of polygeneration (e.g. CHP) and efficient conversion units (e.g. HP) raises the need of including thermal power flows during the design problem formulation. Indeed, space heating (SH) and domestic hot water (DHW) demands represent the largest share of the residential energy requirements [6], illustrating the strong interest of appropriate sizing and control of both the thermal and electrical subsystems.

2.1. State of the Art

The problem of optimal DER systems operation and sizing has been extensively addressed in literature [4–11]. In particular, a large number of studies propose to tackle the optimization problem implementing two main approaches: (i) a *simultaneous* or a (ii) *two-step* [1] method.

In (i), a superstructure-based MILP model is established in order to simultaneously solve the optimal control strategy and design configurations of the different DERs. The following method has been proven particularly suited for the considered design problem [12], in addition of providing the advantage of applying deterministic algorithms to solve the problem formulation. Ashouri et al. [5] proposed a modular and robust framework to minimize the total annualized DER system expenses for buildings. The authors applied a variable electricity tariff generated from the spot market price and the grid utilization factor to

---

[1]i.e *hybrid*

steer consumption towards low demand periods. Steen et al., [7] introduced a multi-layer thermal storage model in order to improve the self-discharging estimation of thermal storage units and utility integration during the design procedure. During (ii), the problem resolution is decoupled into two specific layers: the sizing and the system operation layer. Weber et al., [8] presented a hybrid multi-objective optimisation approach to size a SOFC cogeneration utility for office building use, minimizing both the total annualized cost and environmental impact of the fuel cell. The authors in [6] and [9] extended the latter framework by including additional DER technologies such as HPs, natural gas powered CHP and storage units (i.e. hot water tanks and battery stacks).

Despite introducing innovative and detailed frameworks, the aforementioned models solely targeted specific problems for DER system design, mainly related to economic and environmental objectives from the consumer perspective. A holistic sizing method including a sustainable and efficient self-consumption indicator has yet not been proposed to the best of the author's knowledge. Hence, this paper contributes the state of art by introducing a novel optimal design and operation approach for building energy systems by considering the mentioned challenges. In order to study the current potential of DER systems, typical utilities are modelled and analysed through a hybrid optimization approach. The paper is structured as follows: Section II presents the mathematical models and parameter values of the different DER systems investigated in this study. Section III describes the multi-objective optimization algorithm applied throughout the case studies. In Section IV the simulation results are presented and discussed while Section V finally provides concluding comments about the proposed design method.

3. System Modelling

The system considered throughout this study, presented in Figure 1, consists of a residential building (H) which includes several conversion and storage units $(u \in H)$ to satisfy the different service needs: SH, DHW preparation and electricity consumption. The thermal energy demands are directly delivered by the respective hot-water storage tanks, the outlet flow temperatures being set in regard to the specific heating requirement. In the system configuration (a), an air/water HP extracting heat from the environment T_{out} is used to supply the water tanks. In order to ensure the thermal service provision during peak demand periods, the storage units are equipped with an additional electrical heater. In (b), the thermal energy requirements are satisfied through the means of a NG-fired cogeneration engine.

The building energy management system is based on model predictive control (MPC) which has been identified as an appropriate methodology for this problem formulation [13, 14]. The building regulator hence computes the optimal input variable values for each time step, k of the defined control horizon, n_k. In this case, the predicted operation strategy relies on the following DER systems set points:

(i) The conversion units loads in both configurations
   a. HP input power $\dot{\mathbf{E}}^{+}_{hp,k}$
   b. CHP fuel inlet mass flow $\dot{\mathbf{m}}^{+}_{NG,k}$

(ii) The SH tank charging $\dot{\mathbf{Q}}^{+}_{bat,k}$ and discharging load $\dot{\mathbf{Q}}^{-}_{bat,k}$

(iii) The battery charging $\dot{\mathbf{E}}^{+}_{bat,k}$ and discharging load $\dot{\mathbf{E}}^{-}_{bat,k}$

The controller performance indicator applied throughout this study relies on the building energy system daily operating costs while considering specific comfort and service constraints (section 4.2). The optimization problem solved by the predictive regulator is based on a MILP formulation as follows:

$$
\begin{aligned}
\min_{\mathbf{x},\mathbf{y}} \quad & c^{T}\mathbf{x} + c^{T}\mathbf{y} \\
\text{subject to} \quad & A_1\mathbf{x} + A_2\mathbf{y} \leq b \\
& l \leq \mathbf{x} \leq u, \ \mathbf{y} \in (0,1)
\end{aligned}
\tag{1}
$$

where $\mathbf{x}$ represents the vector of continuous variables, $\mathbf{y}$ the set of integer variables, $A_{1,2}$ the coefficient matrices and (b,l,u) vectors of defined parameters. The following section describes the different control-oriented MILP models of the domestic DER systems analysed in this study and thus included in Eq. 1.

3.1. Building

In order to model the thermal behaviour of the building, a typical resistance-capacitance (RC) structure is used. As discussed in [15], a first-order 1R1C network provides a good description of the building thermal capacity while remaining simple and thus, a similar model has been selected in this study. The construction is thus lumped into a single temperature zone of heat capacitance C_{build}. The building temperature transient can thus be described by the following differential equation:

$$
C_{build}\frac{\mathrm{d}T(t)}{\mathrm{d}t} = \frac{1}{R_{build}}(T(t) - T_{out}(t)) + \dot{Q}^{+}(t)_{build}
\tag{2}
$$

where T_{out} and T are the outdoor and interior temperatures respectively, the parameters R_{build} is the thermal resistances between both temperature zones and $\dot{Q}^{+}_{build}$ represents the net heat load supplied to the building. Regarding the different thermal loads considered within the dwelling, $\dot{Q}^{+}_{build}$ can be further decomposed into the following elements:

$$
\dot{Q}^{+}_{build}(t) = \dot{Q}^{+}_{hs}(t) + A_{build}I^{+}(t)
\tag{3}
$$

where $\dot{Q}^{+}_{hs}$ is the heat provided by the SH storage tank and A_{build} is the effective window area. The values and units of the parameters correspond to the Swiss Society of Engineers and Architect (SIA) norm 380/1 [16] while time-related values have been identified by [17]. It is worth mentioning that, as discussed by the authors of [18], a more accurate description of the dynamics of the building temperature could be achieved though the means of a multiple order model and
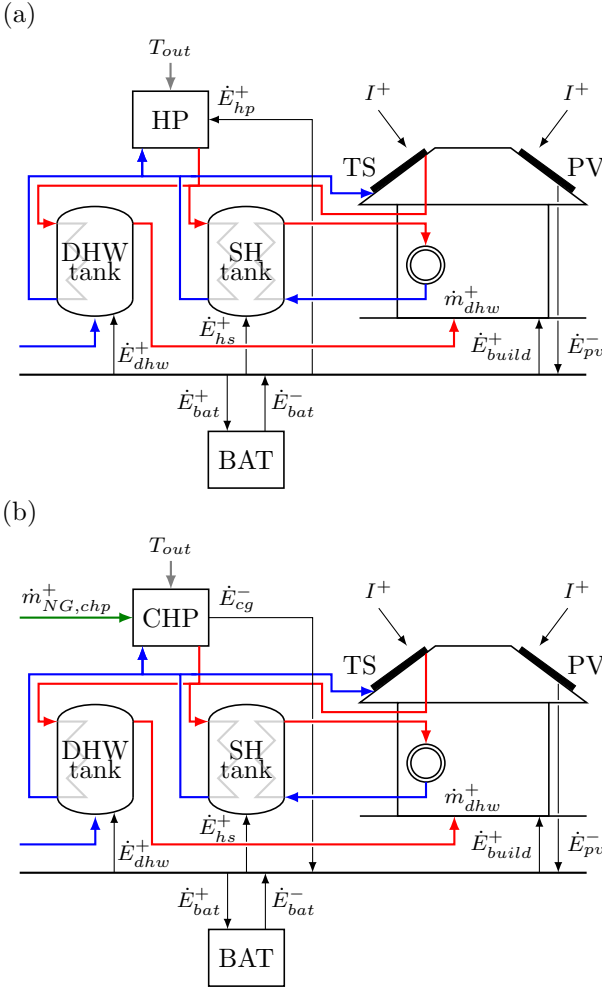
(a)

(b)

Figure 1: System configurations with (a) an air-water heat pump and (b) a cogeneration unit

thus, accounting for the different thermal transients of the building envelope and air [15]. However, since the main focus of this study is on analysing the lumped thermal capacity of the dwelling over daily and seasonal variations rather than a detailed analysis of the temperature response on a short time-scale, the first 1R1C order model is applied. Finally, the supply and return temperatures of the hydronic space heating system (i.e. T_{build}^{supply} and T_{build}^{return} respectively) are defined regarding the building type and construction year as presented in [17]:

$$\mathbf{T}_{build,k}^{supply} = k_1^{supply} - k_2^{supply}(T_{build}^{ref} - \mathbf{T}_{out,k}) \tag{4}$$

$$\mathbf{T}_{build,k}^{return} = k_1^{return} - k_2^{return}(T_{build}^{ref} - \mathbf{T}_{out,k}) \tag{5}$$

3.2. Thermal storage

The thermal energy storage model is based on the formulation introduced by [19] and further developed by [20]; the hot water tank is discretized into n_l virtual storages layers with fixed temperatures, regarding the storage operating range. The water can be shifted between the different temperature layers (l) through heat exchange with an external unit. Therefore, considering a constant c_p value, a heat supply $\dot{Q}_l^h$ to the virtual tank layer l is represented as a hot stream flowing from T_l to T_{l-1}, the mass flow $\dot{m}_l^h$ being the extensive control variable (Eq. 15a). Respectively, a heat delivery $\dot{Q}_l^c$ is expressed as a cold stream entering T_l from the lower temperature level T_{l-1}, of mass flow $\dot{m}_l^c$ (Eq. 15b).

In order to account for tank heat losses $\dot{Q}_l^{loss}$, the thermal load is modelled as a mass flow $\dot{m}_l^{loss}$ from T_l to T_{l-1}. Thus, Equation 15c relates the losses of each layer l to the difference of the respective temperature T_l and the ambient tank conditions T_b, the virtual storage wall surface A_l (Eq. 15d) and the tank specific heat transfer coefficient U_u. In regard to the latter definition, the first storage layer temperature T_1 is considered to be at the surrounding temperature T_b to avoid losses at the bottom layer. Additionally, Equation 6e limits the virtual tank mass to the fixed maximum value while Equation 6f defines the total volume in function of the height-to-diameter ratio π_{HD} and the tank diameter d^d, the design parameter of the thermal storage unit.

For [$u = hs, dhw, l \in [2, n_l], k \in [1, n_k]$]:

$$\dot{\mathbf{Q}}_{u,l,k}^c = \dot{\mathbf{m}}_{u,l,k}^c c_p(T_l - T_{l-1}) \tag{6a}$$

$$\dot{\mathbf{Q}}_{u,l,k}^h = \dot{\mathbf{m}}_{u,l,k}^h c_p(T_l - T_{l-1}) \tag{6b}$$

$$\dot{\mathbf{Q}}_{u,l,k}^{loss} = \dot{\mathbf{m}}_{u,l,k}^{loss} c_p(T_l - T_{l-1}) = \mathbf{A}_{u,l,k} U_u(T_l - T_b) \tag{6c}$$

For [$u = sh, l \in [1, n_l], k \in [1, n_t]$]:

$$\mathbf{A}_{u,l,k} = \frac{\mathbf{m}_{u,l,k}}{\rho(d_u^d/4)} \tag{6d}$$

$$\sum_l \mathbf{m}_{u,l,k} = m_u^{max} = \frac{\pi_{HD}\pi\rho_{wat}(d_u^d)^3}{4} \tag{6e}$$

$$\sum_l \mathbf{A}_{u,l,k} = \pi_{HD}\pi(d_u^d)^2 \tag{6f}$$

The mass balance for the different temperature layers l, at each time step k are thus expressed as follows:

For $[u = hs, l \in [2, n_l - 1], k \in [1, n_k - 1]]$:

$$\mathbf{m}_{u,l,k+1} = \mathbf{m}_{u,l,k} + \big[(\dot{\mathbf{m}}^c_{u,l,k} + \dot{\mathbf{m}}^h_{u,l+1,k} + \dot{\mathbf{m}}^{loss}_{u,l+1,k})$$
$$- (\dot{\mathbf{m}}^c_{u,l+1,k} + \dot{\mathbf{m}}^h_{u,l,k} + \dot{\mathbf{m}}^{loss}_{u,l,k})\big]\mathrm{d}k \tag{7a}$$

$$\mathbf{m}_{u,1,k+1} = \mathbf{m}_{u,1,k} + (\dot{\mathbf{m}}^h_{u,2,k} + \dot{\mathbf{m}}^{loss}_{u,2,k} - \dot{\mathbf{m}}^c_{u,2,k})\mathrm{d}k \tag{7b}$$

$$\mathbf{m}_{u,n,k+1} = \mathbf{m}_{u,n,k} + (\dot{\mathbf{m}}^c_{u,n-1,k} + \dot{\mathbf{m}}^{loss}_{u,n,k} - \dot{\mathbf{m}}^h_{u,n,k})\mathrm{d}k \tag{7c}$$

Here, in the case of Equation 7b, the bottom layer mass in the next time step $k + 1$ is computed from the actual state k to which the mass flow related to the (i) heat losses and (ii) the heat discharge (i.e. hot stream) of next upper layer (i.e. $l = 2$) are added while the mass flow corresponding to a (iii) heat charge (i.e. cold stream) is subtracted. The corresponding mass transfer rates are represented in Figure 2 through (i) red, (ii) green and (iii) blue arrows respectively, between $l = 1$ and $l = 2$. Regarding the different delivery types (i.e. mass/heat) related to the thermal services, additional elements need to be included. Indeed, Figure 2 presents both tank configurations considered in this study, with respect to their application: (a) SH and (b) DHW. In (b), the mass flows related to the cold, fresh water inlet $\dot{\mathbf{m}}_{wat_{fresh},k}$ and DHW outlet $\dot{\mathbf{m}}_{wat,l,k}$ for each temperature layer l, need to be included in the mass balance expression of Equations 7a-7c. Moreover, since no heat delivery is occurring for this tank configuration, the DHW mass balance is defined as follows:

For $[u = dhw, l \in [2, n_l - 1], k \in [1, n_t - 1]]$:

$$\mathbf{m}_{u,l,k+1} = \mathbf{m}_{u,l,k} + \big[(\dot{\mathbf{m}}^c_{u,l,k} + \dot{\mathbf{m}}^{loss}_{u,l+1,k}) -$$
$$(\dot{\mathbf{m}}^c_{u,l+1,k} + \dot{\mathbf{m}}_{wat,n,k} + \dot{\mathbf{m}}^{loss}_{u,l,k})\big]\mathrm{d}k \tag{8a}$$

$$\mathbf{m}_{u,1,k+1} = \mathbf{m}_{u,1,k} + (\dot{\mathbf{m}}_{wat_{fresh},k} + \dot{\mathbf{m}}^{loss}_{u,2,k} - \dot{\mathbf{m}}^c_{u,2,k})\mathrm{d}k \tag{8b}$$

$$\mathbf{m}_{u,n,k+1} = \mathbf{m}_{u,n,k} + (\dot{\mathbf{m}}^c_{u,n-1,k} + \dot{\mathbf{m}}^{loss}_{u,n,k} - \dot{\mathbf{m}}_{wat,n,k})\mathrm{d}k \tag{8c}$$

Additionally, since the DHW distribution network requires a minimum supply temperature $T^{min}_{dhw} = T_j$, no water delivery is performed below this threshold (Eq. 9a) Finally, an electrical backup heater is implemented into each vessel type to provide additional heating capacity during peak consumption hours (Eq. 9b).

For $[u = \{hs, dhw\}, \forall k]$:

$$\dot{\mathbf{m}}_{wat,l,k} = 0 \qquad\qquad l \in [1, j] \tag{9a}$$

$$\dot{\mathbf{Q}}^c_{u,l,k} + \eta_u \dot{\mathbf{E}}^+_{u,l,k} = \dot{\mathbf{m}}^c_{u,l,k} c_p (T_l - T_{l-1}) \qquad\qquad l \in [2, n_l] \tag{9b}$$
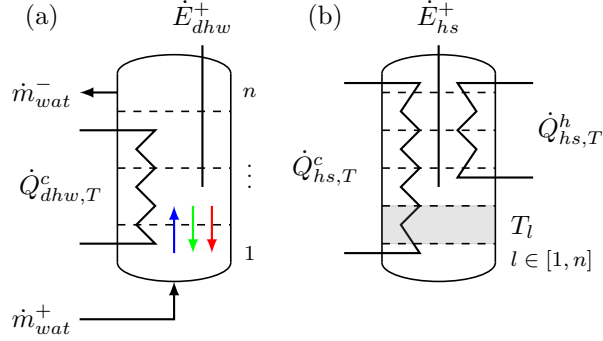
Figure 2: (a) DHW and (b) SH storage tank models

3.3. Electrical storage

The electrical storage unit considered in this study is composed of Li-Ion battery stack which are increasingly targeting the household market segment. The model relies on a simple linear formulation proposed by [21]:

For $[u = bat]$:

$$\mathbf{E}_{u,k+1} = \alpha_u \mathbf{E}_{u,k+1} + (\eta_{u,ch}\dot{\mathbf{E}}^+_{u,k} - \frac{1}{\eta_{u,dis}}\dot{\mathbf{E}}^-_{u,k})\mathrm{d}t \qquad k \in [2, n_k] \qquad (10a)$$

$$\gamma_u^{min} E_u^{size,d} \leq \mathbf{E}_{u,k} \leq \gamma_u^{max} E_u^{size,d} \qquad\qquad \forall k \qquad (10b)$$

where the parameters η_{dis} and η_{ch} represent the dis- and charging efficiencies respectively, while α is the self-discharging ratio of the storage system. In order to neglect the premature deterioration of the stack due to deep discharging cycles and thus, avoid non-linearities, the state of charge (SoC) should remain between 20 and 80 % of the battery rated capacity $E_{bat}^{size,d}$ (Eq. 10b) [22], the design variable of the electrical unit. Similarly, as discussed by the authors of [21], charging/discharging efficiencies are in general state-dependant variables $\eta(\mathbf{E}_{bat})$; however in this study, the aforementioned values are assumed constant to achieve a linear control model.

3.4. Heat pump

Air-source, variable speed heat pumps are a flexible and highly efficient mean to provide heat for low temperature applications, such as SH and DHW preparation. Equation 11a defines the HP performances on the basis of the theoretical coefficient of performance (COP^{ideal}) and an efficiency factor $\boldsymbol{\eta}_{u,l,k}$ to reflect the real system COP [17]. Indeed, the latter parameter significantly varies with heat source/sink temperature fluctuations and hence, has been approximated by a piecewise linear function (Eq. 11b) consisting of $n_i = 9$ intervals. The different coefficients ($\mathbf{a}_l^i$, $\mathbf{b}_l^i$) were fitted from data of 32 air-water heat pump models commercially available. Additionally, in order to optimize the unit output conditions with respect to the different temperature levels of the thermal
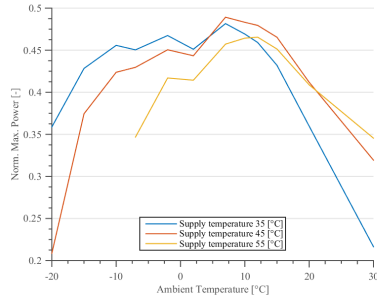
9

service requirements, the generated heat $\dot{\mathbf{Q}}^-_{u,l,k}$ at each time step k is further discretized into n_l outlet temperature levels l. Finally, Equation 11c constrains the the variable speed HP to operate in the upper load range, hence avoiding strong losses due to low compressor speed.
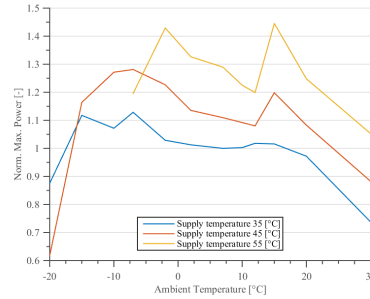
For $[u = hp, l \in [1, n_l], k \in [1, n_k]]$:

$$.\dot{\mathbf{Q}}^-_{u,l,k} = \boldsymbol{\eta}_{u,l,k}\mathbf{COP}^{ideal}_{u,l,k}\dot{\mathbf{E}}^+_{u,l,k} \tag{11a}$$

$$\boldsymbol{\eta}_{u,l,k} = \mathbf{a}^i_l + \mathbf{b}^i_l\mathbf{T}_{out,k} \qquad \mathbf{T}_{out,k} \in [T^{min}_i, T^{max}_i] \tag{11b}$$

$$\gamma_u\dot{E}^{size,d}_u \leq \sum_{l=1}^{n}\dot{\mathbf{E}}^+_{u,l,k} \leq \dot{E}^{size,d}_u \tag{11c}$$

(a) Second law efficiency (b) Maximal power input

Figure 3: Piecewise efficiency and power rating approximation

3.5. CHP engine

The CHP unit considered in this study consists of a NG-powered Stirling cycle, commercially available for residential application [14]. The control-oriented model implements a minimum part-load threshold in order to avoid significant efficiency variations occurring at lower power outputs. Equations 12a-12d state the system performances applying a single piece, linear efficiency function and thus, steering the regulator towards the upper set point range.

For $[u = cg, k \in [1, n_k]]$:

$$\dot{\mathbf{Q}}^-_{u,k} = \dot{Q}^{min}_u + \eta^{heat}_u\dot{\mathbf{m}}^{pw}_{u,NG,k} \tag{12a}$$

$$\dot{\mathbf{E}}^-_{u,k} = \dot{E}^{min}_u + \eta^{elec}_u\dot{\mathbf{m}}^{pw}_{u,NG,k} \tag{12b}$$

$$\dot{\mathbf{m}}^+_{u,NG,k} = \dot{m}^{min}_u + \dot{\mathbf{m}}^{pw}_{u,NG,k} \tag{12c}$$

$$\gamma_u\dot{E}^{size,d}_u \leq \dot{\mathbf{E}}^-_{u,k} \leq \dot{E}^{size,d}_u \tag{12d}$$

Finally, the system is constrained to operate for a minimum time to avoid the premature deterioration of the CHP engine, mainly related to high cycling rates.

The resulting block continuity is expressed as follows:

For $[u = cg]$:

$$\boldsymbol{\sigma}_{u,1} = \mathbf{y}_{u,1} \tag{13a}$$

$$\boldsymbol{\sigma}_{u,k} \leq 1 - \mathbf{y}_{u,k-1}, \boldsymbol{\sigma}_{u,k} \leq \mathbf{y}_{u,k}, \boldsymbol{\sigma}_{u,k} \geq \mathbf{y}_{u,k} + (1 - \mathbf{y}_{u,k-1}) - 1 \tag{13b}$$

$$\sum_{j=k}^{\min(k+\beta_u-1,n_t)} \mathbf{y}_{u,j} - \beta_u \leq -(1 - \boldsymbol{\sigma}_{u,k}) \tag{13c}$$

where $\mathbf{y}_{u,k}$ is a binary variable indicating the unit status (on/off), $\boldsymbol{\sigma}_{u,k}$ represents the CHP system sequence start while β_u is the minimum operating time.

3.6. Photovoltaic system

As presented by [23, 24], a simple and accurate linear model is applied for the photovoltaic (PV) system. The electrical power generation of the PV system $\dot{\mathbf{E}}_{pv,k}^{-}$ is therefore defined using the panel efficiency $\boldsymbol{\eta}_{pv,k}$, the incident solar radiance $\mathbf{I}_k^{+}$ and the total panel surface A_{pv}^d, the unit design variable (Eq. 14a). Furthermore, Equations 14b and 14c define the temperature-dependant efficiency as function of the system technical specifications[2] and the outer temperature $\mathbf{T}_{out,k}$.

For $[u = pv, k \in [1, n_k]]$:

$$\dot{\mathbf{E}}_{u,k}^{-} = A_u^d \boldsymbol{\eta}_{u,k} \mathbf{I}_k^{+} \tag{14a}$$

$$\boldsymbol{\eta}_{u,k} = \eta_{u,ref} - \pi_u (\mathbf{T}_{u,k} - T_{u,ref}) \tag{14b}$$

$$\mathbf{T}_{u,k} = \frac{U_u \mathbf{T}_{out,k}}{U_u - \pi_u \mathbf{I}_k^{+}} - \frac{\mathbf{I}_k^{+}(f_u - \eta_{u,ref} - \pi_u T_{u,ref})}{U_u - \pi_u \mathbf{I}_k^{+}} \tag{14c}$$

3.7. Thermal solar collector

Similarly to the model presented in the previous section, the generated heat of the thermal solar collector is determined by applying the panel efficiency $\boldsymbol{\eta}_{ts,l,k}$, the incident angle modifier β_{IAM}, the incident solar radiance $\mathbf{I}_k^{+}$ and the multiplication factor $\mathbf{f}_{ts,l,k}$ (Eq. 15a); the latter positive value is bounded by the total panel surface A_{ts}^d, the unit design variable (Eq. 15d). In order to integrate the unit output in regard to the different temperature levels of the thermal service demands, the outgoing heat $\dot{\mathbf{Q}}_{ts,l,k}^{-}$ is discretized into n_l inlet and outlet temperature intervals l. Based on the model defined by [25], the system efficiency is defined through the means of the logarithmic mean panel

---

[2]i.e. the thermal transmission coefficient U_{pv}, the temperature coefficient of efficiency π_u, the solar inlet fraction f_{pv} and the reference efficiency and temperature $(\eta_{pv,ref}, T_{pv,ref})$

temperature (15b) and measured constant parameters (15c).

For $[u = ts, l \in [1, n_l], k \in [1, n_k]]$:

$$\dot{\mathbf{Q}}_{u,l,k}^- = \beta_{IAM} \mathbf{f}_{u,l,k} \boldsymbol{\eta}_{u,l,k} \mathbf{I}_k^+ \tag{15a}$$

$$\boldsymbol{\eta}_{u,l,k} = \eta_{u,0} - a_{u,0} \frac{T_{lm} - \mathbf{T}_{out,k}}{\mathbf{I}_k^+} - a_{u,1} \frac{(T_{lm} - \mathbf{T}_{out,k})^2}{\mathbf{I}_k^+} \tag{15b}$$

$$T_{lm} = \frac{T_{l+1} - T_l}{\ln(T_{l+1}/T_l)} \tag{15c}$$

$$\sum_{l=1}^{n_l} \mathbf{f}_{u,l,k} \leq A_u^d \tag{15d}$$

3.8. Mass and energy balances

In order to link the different DER systems to the different service requirements, the building total energy and mass balances are finally defined. Therefore, the utilities (i.e. electricity & natural gas) energy and mass balances can be written as follows:

$$\sum_u \dot{\mathbf{E}}_{u,k}^+ - \sum_u \dot{\mathbf{E}}_{u,k}^- + \dot{\mathbf{E}}_{build,k}^+ = \dot{\mathbf{E}}_{grid,k}^+ \qquad u \in H, k \in [1, n_k] \tag{16}$$

$$\sum_u \dot{\mathbf{m}}_{NG,u,k}^+ = \dot{\mathbf{m}}_{NG,grid,k}^+ \qquad u \in H, k \in [1, n_k] \tag{17}$$

where $\dot{\mathbf{E}}_{grid}^+$ and $\dot{\mathbf{m}}_{NG,grid}^+$ represent the net electricity and natural gas imports from the local distribution grid respectively. Regarding the different temperature levels corresponding to the thermal service demands and the respective DER system outputs, heat cascading is performed to optimally selected the unit operating set points [8, 17, 20]. The method consists of splitting the aggregated heat load of the cold $\dot{\mathbf{Q}}^c$ and hot $\dot{\mathbf{Q}}^h$ streams (i.e. streams to be heated and cooled respectively) into several temperature intervals n_l and computing the residual heat $\dot{R}_l$ cascaded down to the next lower interval $l-1$ as defined in Eq. 18.

For $[u \in H, k \in [1, n_k]]$:

$$\sum_{i=1}^{n_{l,h}} \dot{\mathbf{Q}}_{u,i,k}^h - \sum_{j=1}^{n_{l,c}} \dot{\mathbf{Q}}_{u,j,k}^c + \dot{R}_{l+1} - \dot{R}_l = 0 \quad l \in [1, n_l]$$

$$\dot{R}_l \geq 0 \qquad\qquad\qquad l \in [2, n_l] \tag{18}$$

$$\dot{R}_1 = \dot{R}_{n_l+1} = 0$$

Finally, the mass balance regarding the DHW requirements is expressed in Eq. 19, j being the temperature index which corresponds to the minimum supply temperature of the latter service (i.e. 323 [K]).

$$\sum_{l=j}^{n} \dot{\mathbf{m}}_{wat,l,k}^- = \dot{\mathbf{m}}_{dhw,k}^+ \qquad k \in [1, n_k] \tag{19}$$

3.9. Cyclic conditions

The cyclic constraints impose that the SoC conditions of the different storage units at the first time step k are equal to the conditions of the succeeding day time step $k + n$. The latter formulation avoids strong self-discharge losses resulting from long-term storage, hence improving the system efficiency and operating costs [14]. Moreover, since large-scale storage units require substantial investments, space and complex management systems, residential buildings are not suited to perform seasonal storage. Equations 20a and 20b determine the cyclic constraints for the electrical and thermal storage units respectively, j representing the minimum supply temperature level of the heat tanks.

$$\mathbf{E}_{bat,k} = \mathbf{E}_{bat,k+n} \qquad\qquad k \in [1, n_k] \quad (20a)$$

$$\sum_{l=1}^{n} \mathbf{Q}_{u,l,k} = \sum_{l=1}^{n} \mathbf{Q}_{u,l,k+n} \qquad\qquad u \in [hs, dhw], k \in [1, n_k] \quad (20b)$$

4. Methodology

The proposed sizing algorithm relies on a *hybrid* resolution method, thus decoupling the problem into two layers (Figure 4). The upper layer (master) uses an evolutionary MOO to solve the optimal design problem while the lower layer (slave) solves the optimal control (i.e. though MPC) strategy, relying on a MILP formulation. The choice of applying a decoupled, heuristic-based optimization approach over a deterministic method can be summarized as follows:

1. Evolutionary algorithms screen the whole search space, hence providing more information to analyse the trade-off between conflicting objectives.
2. The latter methodology is a robust approach which features the capability of dealing with non-linearities, particularly regarding the objectives, and highlighting the location of discontinuities.
3. Since the target is to provide decision support for an engineering issue, the latter approach enables the selection of a final solution among a set of optimal combinations by considering different criteria (e.g. financial) [19].

During the design process, the optimal control is assumed to achieve a perfect realization (i.e. no prediction errors) and hence, the lower optimization layer solely solves a single operation strategy per horizon period n_k at $k = 1$.
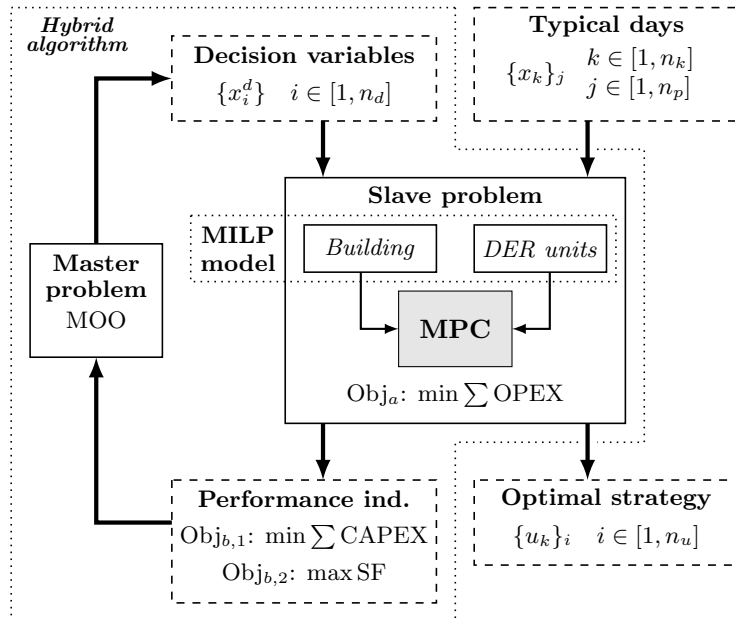
Figure 4: Design algorithm

4.1. Data clustering

Regarding the computational complexity related to the resolution of the aforementioned optimization problem, data clustering has been performed. Indeed, input data of urban DER design procedures is commonly defined through the means of a typical reference year, assumed constant over the entire energy systems lifetime ($\simeq 25$ years) [20]. However, since the latter number of operating periods remains significant, the annual data set is further decreased. For this purpose, a *k-medoid* clustering method has thus been implemented; the deterministic approach identifies the different cluster centres based on the smallest sum of distances within the cluster [26]. The cluster size is selected based on specific performance indicators presented by the author of [20]:

- Silhouette coefficient s

- Mean squared and absolute error (MSE-MAE)

- Percentage errors (PE)

- Relative per dimension total and peak errors

In order to limit the number of data dimensions and hence generate consistent cluster results, solely two input parameters have been considered during the clustering process: (i) the ambient temperature T_{out} and (ii) the global solar irradiation $\dot{I}^+$. The remaining consumption (electricity, domestic hot water)

14

and tariff (electricity, natural gas) data is then defined *a posteriori* through the means of the computed cluster centres.

As presented in Table 1, all performance indicators improve with the increasing of cluster numbers k. It is observed that the silhouette coefficient which defines the cohesion of structure rapidly decreases below the limit of 0.5 while remaining above the inconsistency threshold of 0.25 [26]. Nevertheless, as discussed by [20], the aforementioned values have been proposed for bi-dimensional data set while the considered case solves a 48-dimensional (2 parameters of 24 hours) problem. The analysis of dimension relative errors reveals that peak errors are a critical selection criteria; the *k-medoids* method indeed selects the best day out of the cluster with respect to the global performance although it might not represent well a specific dimension. With regard to these results, the cluster size $n_p = 18$ appears to provide the best trade-off between the different quality factors and the resulting input data set.

Table 1: Clusters performance indicators

| | **Global Indicators** | | | | **Temperature** | | **Solar radiance** | |
k	s	MSE	MAE	PE	Max err. [%]	Err. [%]	Max err. [%]	Err. [%]
2	0.66	0.49	0.47	-0.01	44.68	3.82	60.17	-2
3	0.54	0.29	0.32	-0.03	36.78	-3.30	59.96	-2.63
4	0.48	0.24	0.27	-0.02	36.78	0.55	56.2	-1.74
5	0.47	0.14	0.16	-0.04	34.04	-0.03	56.41	-4.24
15	0.33	0.02	0.03	-0.03	22.49	-0.02	49.00	-3.06
16	0.31	0.02	0.03	-0.03	22.49	-0.08	49.00	-2.76
17	0.33	0.03	0.04	-0.03	20.06	0.15	42.23	-3.14
18	0.33	0.05	0.07	-0.02	20.06	-0.41	41.92	-2.29
19	0.30	0.06	0.07	-0.03	20.06	-0.21	42.23	-3.03
20	0.29	0.06	0.07	-0.02	20.06	-0.08	42.23	-2.31

This choice is indeed validated through *two* specific approaches:

- The *graphical* representation of Figure 5 and Figure 6 revealing the load curve of both the typical annual data and the cluster values for each input parameter. As discussed previously, the solar irradiation and temperature extreme values are less represented; however, regarding there low frequency of a few hours per annum, the latter can be neglected without inducing any substantial quality losses.

- Indeed, Table 2 details the relative load differences between the MPC operation over the entire annual data set and the selected periods weighted by there respective frequency, considering a perfect realization for different DER system configurations. The results vary from 0.08 to 3.89 % which

remains within the global and dimensional indicator value range of Table 1 and thus, provide a strong *numerical* validation of the cluster selection.

Table 2: Numerical cluster selection validation

System†		Load Errors			
PV [m^2]	El. st. [kWh]	Imp. [%]	Exp. [%]	Prod. [%]	Cons. [%]
0	3	2.48	-	-	2.26
50	3	1.74	0.74	2.26	2.87
100	5	0.74	0.26	3.49	3.89
200	7	0.08	1.87	2.26	1.75

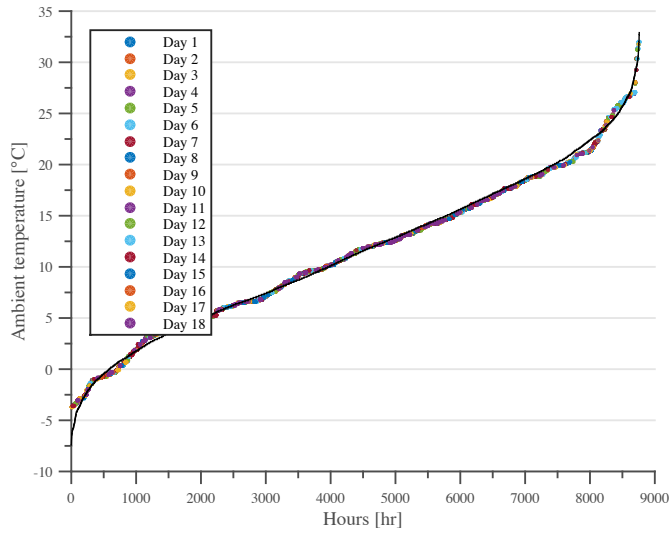†Fixed thermal storage of 23 kWh$_{th}$ and HP of 3 kW$_{el}$

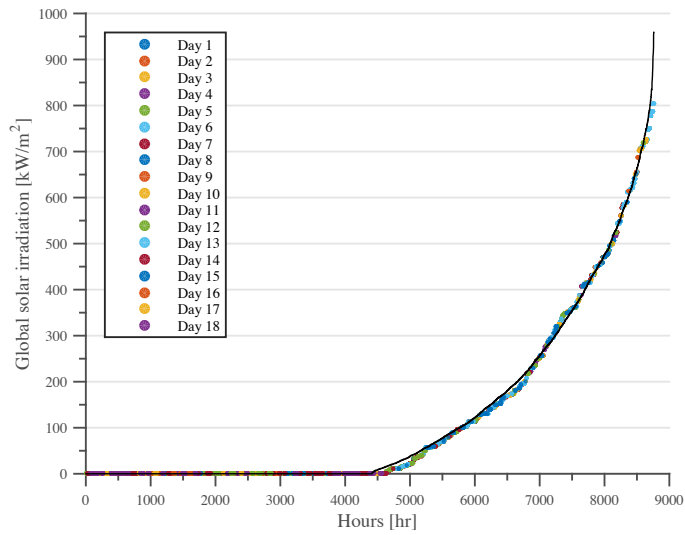Figure 5: Annual load curves of the temperature profile

Figure 6: Annual load curves of the global solar irradiation profile

4.2. Objectives

From the building perspective, cost-based demand response is applied and thus, the local MPC controller minimizes the operating expenses in addition to the comfort penalty cost [14]. The perceived penalty is linearly proportional to the temperature difference between the comfort range $[T^{min}, T^{max}]$ and the indoor temperature T, multiplied by the weighting factor M to prioritize comfort. The energy system operating cost are expressed as the sum of the NG consumption

of the cogeneration unit (case b) combined to the expenses of the electricity imports and subtracted by the power export revenues. In order to promote self-consumption, the feed-in tariff $\mathbf{c}_{el,i}^-$ is set below the standard day-night tariff $\mathbf{c}_{el,i}^+$ applied in this study.

$$\text{Obj}_a = \sum_{j=1}^{n_p} \mathbf{OPEX}_j \tag{21a}$$

$$= \sum_{j=1}^{n_p} \left(\sum_{i=k}^{k+n_k} \mathbf{c}_{el,i,j}^+ \dot{\mathbf{E}}_{grid,i,j}^+ - \mathbf{c}_{el,i,j}^- \dot{\mathbf{E}}_{grid,i,j}^- + \mathbf{c}_{ng,i,j}^+ \dot{\mathbf{m}}_{NG,grid,i,j}^+ \right)$$

$$+ \sum_{j=1}^{n_p} \sum_{i=k}^{k+n_k} \left(\mathbf{p}_{inf,i,j} + \mathbf{p}_{sup,i,j} \right)$$

$$\mathbf{p}_{inf,i,j} \geq M(T^{min} - \mathbf{T}_{i,j}), \quad \mathbf{p}_{inf,i,j} \geq 0 \qquad \forall i,j \tag{21b}$$

$$\mathbf{p}_{sup,i,j} \geq M(\mathbf{T}_{i,j} - T^{max}), \quad \mathbf{p}_{sup,i,j} \geq 0 \qquad \forall i,j \tag{21c}$$

In the master problem layer, the first objective is minimizing the total capital expenses (Eq. 22) while the second indicators is maximizing the *self-sufficiency* (SS) ratio (Eq. 23) as load matching metric [27]. The latter performance index defines the share of generated power used over the total building electricity consumption where $\mathbf{F}^{1 \times n_k}$ represents the annual cluster frequency vector. The evolutionary algorithm is selecting the values of the n_d decision variables based on the operating strategy defined by the slave problem (i.e MPC). The latter variable set $\{x_j^d\}$ consists of the different DER systems sizes and capacities presented in the previous modelling sections.

$$\text{Obj}_{b,1} = \sum_{j=1}^{n_u} \mathbf{CAPEX}_j = \sum_{j=1}^{n_u} a + b x_j^d \tag{22}$$

$$\text{Obj}_{b,2} = \mathbf{SS} = \frac{\sum\limits_{i=1}^{n_p} \mathbf{F}_i (\mathbf{E}_{prod,i}^+ - \mathbf{E}_{grid,i}^-)}{\sum\limits_{i=1}^{n_p} \mathbf{F}_i (\mathbf{E}_{grid,i}^+ - \mathbf{E}_{grid,i}^- + \mathbf{E}_{prod,i}^+)} \tag{23}$$

5. Results and discussion

In this section, the optimal energy system sizing framework is implemented to define the optimal energy systems sizes and control strategies of different Swiss residential buildings, with a nominal occupancy of 4 people. The effective building surface is fixed to 160 m^2 for single family houses which corresponds to living area of 40 m^2/person. For this study, a standard hourly profile of domestic hot water $\mathbf{m}_{dhw}^+$ (i.e. in average 200 l/day) and the electricity consumption $\mathbf{E}_{build}^+$ (i.e. in average 8.3 kWh/day), have been used and post-processed regarding the clusters definition presented in the previous section.

Table 3: Cost function values

Unit	Param. [u]†	Capital cost			Bounds [u]†	
		a [CHF]	b [CHF/u]†	*Ref.*	Min	Max
HP	$\dot{E}$ [kW]	5680	1240	[28]	1.5	5
CHP	$\dot{E}$ [kW]	0	3800	[29]	1	5
PV	A [m^2]	0	750	[23]	0	160
TS	A [m^2]	0	540	[23]	0	160
SH HS	d [m]	0	985	[20]	0	1
DHW HS	d [m]	0	2300	[20]	0.4	1
BAT	E [kWh]	0	546	[30]	0	10

†Regarding the design parameter unit

The parameter values and cost functions of the different DER system types analysed are exposed in Table 4 and 3 respectively. For all building types investigated, the comfort boundaries presented in Equation 21b-21c are determined as following:

$$T_{min}(t) = \begin{cases} 16 \ [^{\circ}C], & 11 \text{ p.m.} \leq t \leq 7 \text{ a.m.} \\ 20 \ [^{\circ}C], & \text{otherwise} \end{cases}$$

$$T_{max} = 22 \ [^{\circ}C]$$

Figure 7 presents the Pareto front of a single family house (SFH) simulation, constructed in the period ≤ 1920 and equipped with an air-source heat pumps (a). As shown, the second design objective, i.e. the *self-sufficiency* factor (SS), first rapidly increases with the PV array size, before constantly declining while operating expenses continue to decrease. Indeed, regarding the considered problem definition, the SoC of the different storage units are imposed to return to their nominal state at the end of each day (i.e. cyclic condition); thus power imports from the local distribution grid are still required to satisfy the electricity demand during the first morning hours since the maximal storage capacity is limited (Table 3). Figure 7 details an additional front representing the *self-consumption factor* (SC); the latter metric defines the ratio between the used and total generated energy (25). For small PV array sizes, the SC indicator is close to the maximal value since the generated power is directly used on site while for larger system sizes electricity exports to the distribution grid remain mandatory due to the reasons stated previously.

$$\mathbf{SC} = \frac{\sum_{i=1}^{n_p} \mathbf{F}_i(\mathbf{E}^+_{prod,i} - \mathbf{E}^-_{grid,i})}{\sum_{i=1}^{n_p} \mathbf{F}_i(\mathbf{E}^+_{prod,i})} \tag{25}$$

Table 4: Parameter values used in the case study

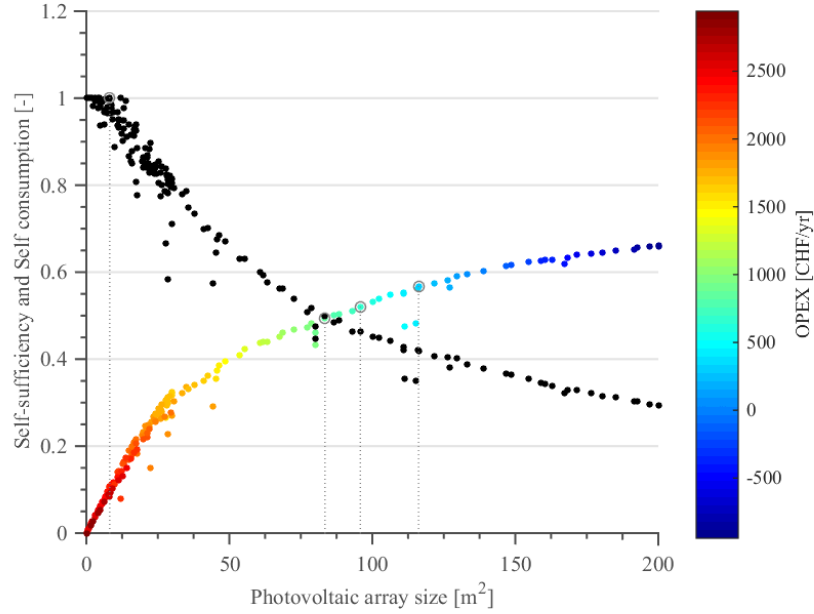| Param.	Value		Param.	Value	
A_{build}	10	[m^2]	$c_{el/ng}^+$	0.23/0.08	[CHF/kWh]
C_{build}	0.11	[MJ/m^2]	$c_{el/ng}^-$	0.1/0.05	[CHF/kWh]
T_{build}^{ref}	263	[K]	n_k	25	[hr]
M	0.4	[CHF/hr·K]	Δk	1	[hr]
$U_{hs/dhw}$	2	[W/m^2·K]	β_{cg}	4	[hr]
$\pi_{HD_{hs/dhw}}$	3	[-]	$\eta_{cg}^{el/th}$	0.29/0.68	[-]
$T_{l_{hs}}$	333-293	($\Delta T_l = 10$) [K]	$\gamma_{cg}^{min/max}$	0.5/1	[-]
$T_{l_{dhw}}$	343-283	($\Delta T_l = 20$) [K]	$\gamma_{hp}^{min/max}$	0.25/1	[-]
α_{bat}	0.99992	[-]	β_{ts}	0.8	[-]
$\eta_{bat,ch/dis}$	0.9	[-]	$\eta_{ts,0}$	0.83	[-]
$\gamma_{bat}^{min/max}$	0.2/0.8	[-]	$a_{ts,0/1}$	3.7/0.009	[-]
$T_{pv,ref}$	298	[K]	f_{pv}	0.9	[-]
$\eta_{pv,ref}$	0.14	[-]	π_{pv}	0.001	[-]

Figure 7: Pareto front of (i) the SF and RER system size in colour plot and (ii) the GM in black

In order to improve the analysis of the consumer benefits of investing in the

RER based energy system size with respect to the grid impact, a grid interaction metric, the *generation multiple* (GM) [27] is introduced, defining the ratio between the imported and exported peak powers over the integration period (Eq. 26). The difference between the aforementioned SS factor and the GM, weighted by the respective factors w_1 and w_2 (Eq. 27), is finally considered. Indeed, since low power generation from small PV arrays strongly improves the SF while slightly affecting the GM, the represented plot first increases until reaching its peak 8.17 [m^2] (for $w_1,w_2 = 1$). Following this point, the difference highly decreases, therefore translating the stronger growth of the GM over the SF with additional investments in the specific RER system. Indeed, in this case, both the distribution grid operator (i) and the consumer (ii) benefits are worsen due to stronger peak power requests (i) and larger annual electricity curtailment losses (ii). The optimum of the presented benefit factor (BF) hence reflects the DER system size corresponding to the maximal economical benefits in view of the consumer interest while engendering grid-friendly operation regarding the limited GM value.

$$\mathbf{GM} = \frac{\max_k \dot{\mathbf{E}}_{grid,k}^-}{\max_k \dot{\mathbf{E}}_{grid,k}^+} \tag{26}$$

$$\mathbf{BF} = w_1\mathbf{SS} - w_2\mathbf{GM} \tag{27}$$

Regrading the energy system configurations considered in this study, Figure 8 represents the additional Pareto fronts of the SS objective for the same building type used during the previous simulation. In the case of (b), the plotted curve begins at the SS value of 0.39 [-] since the CHP engine already contributes for a substantial share of the total power consumption, mainly during heating season. Similar to configuration (a), the SS significantly increases for small system investments before reaching the maximal value of 1 [-]. The third front reflects the case for which all heating requirements (SH and DHW) are provided through the means of flexible electric heaters (resistors) considering a constant first law efficiency η of 0.9 [-]. The SS corresponding to the BF peak value are identified through dotted lines (*opt*) while the respective DER design parameters are reported in Table 9.

The comparison shows that the defined optimal DER system size strongly depends on the conversion unit applied; in case of (b), the SS grows strongly for small investment expenses, mainly related to the CHP and storage capacity increase. The use of PV and CHP systems is indeed a highly attractive combination regarding their specific generation season and hence, solely DER with moderate capacities are necessary to reach the BF maximum. When using standard electric heaters, the optimal unit sizes are exceeding the presented values of configuration (a), mainly related to the low efficiency of the considered heating system. Indeed, during the heating period, the generated power is directly consumed for the different service requirements and thus, large thermal storage capacities are not necessary.
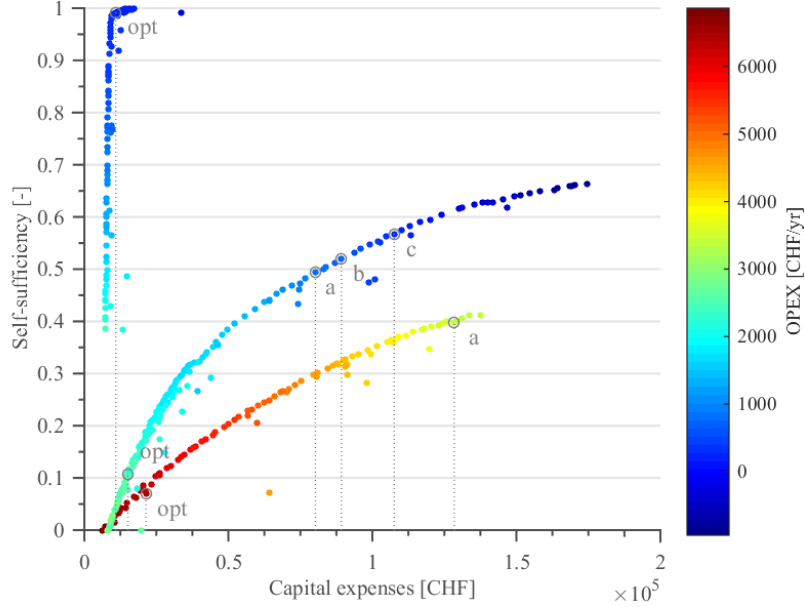
21

Figure 8: Self-sufficiency Pareto front of different energy system configurations (*top*: CHP, *centre*: HP, *bottom*: EL

To compare the proposed configurations to a typical design criterion used in literature, i.e. total self-sufficiency [3, 9, 31], Table 9 enumerates the optimal DER system sizes related to the selected points of Figure 8: a zero-energy building, assuming a perfect (*a*), 80% (*b*) and 55% (*c*) seasonal storage round-trip efficiencies[3]. As expected, when applying electric conversion units, the DER unit sizes corresponding to the different total self-sufficiency assumptions are located well above the benefit factor optimum introduced previously. However, in the case of (b), the zero-energy building metric is achieved without any RER regarding the strong SH and DHW requirements and thus, the resulting high power generation. While the self-sufficient building concept is generally viewed as an economically and environmentally sustainable solution, the latter zero-energy criterion has a substantial impact on the local distribution grid. Figure 10 presents the daily export and generation load curves for both design configurations *opt* and *a* for configuration (a); indeed, electricity exports highly diverge for both cases, feed-in peak differences are reaching over 6 [kW] over noon (GM > 1). Hence, from a power network perspective, self-sufficiency design criteria are rendering conventional grid operation extremely critical and even impossible on a large scale without any extensive overhauling. In case of electric heaters, the energy system sizes required to achieve the total self-sufficiency (*b,c*) objec-

---

[3]Excess electricity generation, mainly related to seasonal variations, is exported and stored by the power network

tives exceed the considered design variable upper limit A_{pv}^d of 160 [m^2] (Table 3), thus showing the unsustainable of using the latter types of conversion units.
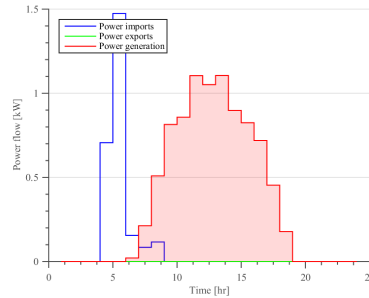
Figure 9: DER system size comparison

DER [u]	**HP**				**CHP**		**EL**	
	$opt^\dagger$	a	b	c	opt	a	opt	a
PV	8.17	83.45	95.81	116.18	0	2.98	14.09	160
TS	0.04	0.01	0	0.17	0	0.09	0.02	0.05
BAT	1.11	9.58	9.4	10	1.54	1.39	8.64	0
Unit	1.85	2.94	3.13	4.5	2.55	2.25	-	-
DHW	0.42	0.53	0.4	0.62	0.49	0.57	0.42	0.42
SH	0.34	0.99	1	1	0.65	0.46	0.15	1

†BF optimum
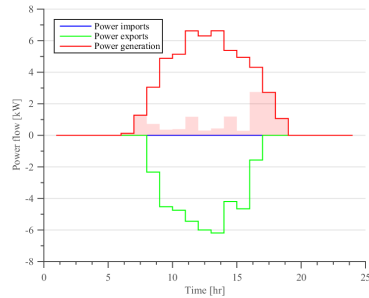
(a) System configuration of point a (b) System configuration of point opt

Figure 10: Daily (30th June) load curves for different system configurations of a SFH equipped with an air-water HP (self-consumption represented by shaded area)

Finally, Table 5 presents the specific DER system sizes when considering different building construction periods. Regarding the results shown, following remarks can be noticed:

- In the case of using a **HP**, the heating unit capacity is slightly varying with the building age. Nevertheless, while the heat storage system substantially decreases for insulated dwellings, the battery stack size increases. This observation might be explained by a primary demand shift from thermal to electric power related to the improvement of the building heat losses. Since the BF indicator is based on the peak electricity export value which occur during summer time, i.e. when electricity consumption is similar for all dwelling types, the optimal PV array sizes remain low (≤ 0.97 [kW$_p$]).

- When applying a **CHP**, the trend is less pronounced; however, the conversion unit capacity grows along with the building heat transmission

coefficient and thus, with the SH requirements. The latter increase engenders an expansion of the storage system sizes in order to recover the excess power/heat generated short demand periods (i.e. due to the minimum running time constraint). Since the CHP unit is already providing an large share of the total electricity demand, the average optimum RER energy based system size is null; the building construction year appears to have no significant impact on the PV capacity.

Table 5: DER system sizes at the BF optimum

	Year	Component [u]						SS/ SC[-]	U [kW/K]
		PV	TS	BAT	HP/CG	DHW	SH		
a	< 1920	8.17	0.04	1.11	1.85	0.42	0.34	0.11/1	0.29
a	1920-80	10.03	0.02	0.91	2.12	0.45	0.63	0.12/0.99	0.32
a	1980-05	6.11	0.02	1.28	1.5	0.47	0.014	0.09/1	0.24
b	< 1920	0	0	1.54	2.55	0.49	0.65	0.99/1	0.29
b	1920-80	0	0	1.88	2.91	0.48	0.69	0.99/1	0.32
b	1980-05	0.02	0	1.65	2.09	0.4	0.44	0.98/0.99	0.24

6. Conclusion

In this paper, the design and control problem of building energy systems has been addressed. For this purpose, a two-level optimization framework has been developed; while the lower layer defines the cost-optimal operation strategy, a heuristic based optimization algorithm identifies the DER configuration values. The system operation relies on a model predictive control formulation for which, control-oriented models of the different energy systems have been defined, using a mixed integer linear programming (MILP) formulation.

The following case studies presented optimal conventional and renewable energy systems configurations for typical buildings with different construction years. The distributed energy systems included in the simulation are batteries, space heating and domestic hot water storage tanks, photovoltaic arrays, thermal collectors, cogeneration engines and air-source heat pumps. The results provided different optimal trade-off unit configurations with respect to the total investment cost and the defined self-sufficiency indicator. In addition, a novel sizing criterion was introduced to define the optimal energy system sizes with regard to the consumer interests while steering towards a grid-friendly operation. The investigations exhibited that proper sizing of both the conversion and storage units strongly affected the impact of RER in residential buildings and the distribution network.

Despite the fact that this study solely considered typical Swiss residential dwellings, the presented framework is also applicable for different building affectations and usage, with individual consumption profiles. Future work includes an extension and additional analysis of this parameter set.

References

[1] A. Bernstein, L. Reyes-Chamorro, J.-Y. L. Boudec, M. Paolone, A composable method for real-time control of active distributionnetworks with explicit power setpoints. Part i: Framework, Electric Power Systems Research 125 (2015) 254–264. `doi:http://dx.doi.org/10.1016/j.epsr.2015.03.023`.

[2] R. Luthander, J. Widén, D. Nilsson, J. Palm, Photovoltaic self-consumption in buildings: A review, Applied Energy 142 (2015) 80–94. `doi:http://dx.doi.org/10.1016/j.apenergy.2014.12.028`.

[3] J. Munkhammar, P. Grahn, J. Wide, Quantifying self-consumption of on-site photovoltaic power generation in households with electric vehicle home charging, Solar Energy 97 (2013) 208–216. `doi:http://dx.doi.org/10.1016/j.solener.2013.08.015`.

[4] S. F. Fux, M. J. Benz, L. Guzzella, Economic and environmental aspects of the component sizing for a stand-alone building energy system: A case study, Renewable Energy 55 (2013) 438–447. `doi:http://dx.doi.org/10.1016/j.renene.2012.12.034`.

[5] A. Ashouri, S. S. Fux, M. J. Benz, L. Guzzella, Optimal design and operation of building services using mixed-integer linear programming techniques, Energy 59 (2013) 365–376. `doi:http://dx.doi.org/10.1016/j.energy.2013.06.053`.

[6] R. P. Menon, M. Paolone, F. Maréchal, Study of optimal design of polygeneration systems in optimal control strategies, Energy 55 (2013) 134–141. `doi:doi:10.1016/j.energy.2013.03.070`.

[7] D. Steen, M. Stadler, G. Cardoso, M. Groissbck, N. DeForest, C. Marnay, Modeling of thermal storage systems in milp distributed energy resource models, Applied Energy 137 (2015) 782–792. `doi:http://dx.doi.org/10.1016/j.apenergy.2014.07.036`.

[8] C. Weber, F. Maréchal, D. Favrat, S. Kraines, Optimization of an sofc-based decentralized polygeneration system for providing energy services in an office-building in tokyo, Applied Thermal EngineeringArticle in Press. `doi:doi:10.1016/j.applthermaleng.2005.05.031`.

[9] G. Kayo, R. Ooka, Building energy system optimizations with utilization of waste heat from cogenerations by means of genetic algorithm, Energy and Buildings 42 (2010) 985–991. `doi:doi:10.1016/j.enbuild.2010.01.010`.

[10] M. Kefayat, A. L. Ara, S. N. Niaki, A hybrid of ant colony optimization and artificial bee colony algorithm for probabilistic optimal placement and sizing of distributed energy resources, Energy Conversion and Management 92 (2015) 149–161. `doi:http://dx.doi.org/10.1016/j.enconman.2014.12.037`.

[11] R. Bornatico, M. Pfeiffer, A. Witzig, L. Guzzella, Optimal sizing of a solar thermal building installation using particle swarm optimization, Energy 41 (2012) 31–37. `doi:doi:10.1016/j.energy.2011.05.026`.

[12] A. Bemporad, M. Morari, Control of systems integrating logic, dynamics, and constraints, Automatica 35 (1999) 407–427.

[13] R. P. Menon, M. Paolone, F. Maréchal, Intra-day electro-thermal model predictive control for polygeneration systems in microgrids, Tech. rep., EPFL (2015).

[14] A. Collazos, F. Maréchal, C. Gähler, Predictive optimal management method for the control of polygeneration systems, Computers and Chemical Engineering 33 (2009) 1584–1592. `doi:doi:10.1016/j.compchemeng.2009.05.009`.

[15] S. F. Fux, A. Ashouri, M. J. Benz, L. Guzzella, Ekf based self-adaptive thermal model for a passive house, Energy and Buildings 68 (2014) 811–817. `doi:http://dx.doi.org/10.1016/j.enbuild.2012.06.016`.

[16] L énergie thermique dans le bâtiment - sia 380/1 (January 2001).

[17] L. Girardin, A gis-based methodology for the evaluation of integrated energy systems in urban area, Ph.D. thesis, EPFL (2012). `doi:doi:10.5075/epfl-thesis-5287`.

[18] F. Sossan, H. Bindner, H. Madsen, D. Torregrossa, L. R. Chamorro, M. Paolone, A model predictive control strategy for the space heating of a smart building including cogeneration of a fuel cell-electrolyzer system, Electrical Power and Energy Systems 62 (2014) 879–889. `doi:http://dx.doi.org/10.1016/j.ijepes.2014.05.040`.

[19] H. Becker, Methodology and thermo-economic optimization for integration of industrial heat pumps, Ph.D. thesis, EPFL (2012). `doi:doi:10.5075/epfl-thesis-5341`.

[20] J. Rager, Urban energy system design from the heat perspective using mathematical programming including thermal storage, Ph.D. thesis, EPFL (2015).

[21] K. Heussen, S. Koch, A. Ulbig, G. Andersson, Energy storage in power system operation: The power nodes modeling framework, in: Innovative Smart Grid Technologies Conference Europe (ISGT Europe), 2010 IEEE PES, 2010. `doi:10.1109/ISGTEUROPE.2010.5638865`.

[22] F. Oldewurtel, A. Ulbig, M. Morari, G. Andersson, Building control and storage management with dynamic tariffs for shaping demand response, in: Innovative Smart Grid Technologies (ISGT Europe), 2011 2nd IEEE PES International Conference and Exhibition, 2011. `doi:10.1109/ISGTEurope.2011.6162694`.

[23] A. Ashouri, Simultaneous design and control of energy systems, Ph.D. thesis, Institute for Dynamic Systems and Control, ETH Zrich (2014). doi:http://dx.doi.org/10.3929/ethz-a-010210627.

[24] B. Sandnes, J. Rekstad, A photovoltaic/thermal (pv/t) collector with a polymer absorber plate. experimental study and analytical model, Solar Energy 72 (2002) 63–73.

[25] J. A. Duffie, W. A. Beckman, Solar Engineering of Thermal Processes, Wiley, 2013.

[26] L. Kaufman, P. J. Rousseeuw, Finding Groups in Data: An Introduction to Cluster Analysis, John Wiley & Sons, Inc, 2005. doi:10.1002/9780470316801.

[27] J. Salom, A. J. Marszal, J. Widén, J. Candanedo, K. B. Lindberg, Analysis of load match and grid interaction indicators in net zero energy buildings with simulated and monitored data, Appplied Energy 136 (2014) 119–131. doi:http://dx.doi.org/10.1016/j.apenergy.2014.09.018.

[28] S. Henchoz, C. Weber, F. Maréchal, D. Favrat, Performance and profitability perspectives of a co2 based district energy network in geneva's city centre, Energy 85 (2015) 221–235. doi:http://dx.doi.org/10.1016/j.energy.2015.03.079.

[29] A. C. Rueda-Medina, J. F. Franco, M. J. Rider, A. Padilha-Feltrin, R. Romero, A mixed-integer linear programming approach for optimal type, size and allocation of distributed generation in radial distribution systems, Electric Power Systems Research 97 (2013) 133 143. doi:http://dx.doi.org/10.1016/j.epsr.2012.12.009.

[30] B. Zakeri, S. Syri, Electrical energy storage systems: A comparative life cycle cost analysis, RenewableandSustainableEnergyReviews 42 (2015) 569–596. doi:http://dx.doi.org/10.1016/j.rser.2014.10.011.

[31] M. Hamdy, A. Hasan, K. Siren, A multi-stage optimization method for cost-optimal and nearly-zero-energy building solutions in line with the epbd-recast 2010, Energy and Buildings 56 (2013) 189–203. doi:http://dx.doi.org/10.1016/j.enbuild.2012.08.023.